Invited Paper

Impact of stochastic process variations on overlay mark fidelity towards the 5 nm node

Mike Adel[a], Roel Gronheid[d], Chris Mack[b], Philippe Leray[c], Evgeni Gurevich[a], Bart Baudemprez[c], Dieter Vandenheuvel[c], Antonio Mani[d], Sharon Aharon[a], Dana Klein[a], Jungtae Lee[e], & Mark D. Smith[f]

[a] KLA-Tencor Israel, 1 Halavyan St. Migdal Ha'emek, 23100, Israel
[b] Fractilia, USA
[c] IMEC, Leuven, Belgium
[d] KLA-Tencor, Belgium
[e] KLA-Tencor, Korea
[f] KLA-Tencor Corporation, USA.

ABSTRACT

In this publication the authors have investigated both theoretically and experimentally the link between line edge roughness, target noise and overlay mark fidelity. Based on previous work[i], a model is presented to explain how any given edge of a printed feature could have a mean position that varies stochastically (i.e., randomly, following a normal distribution) due to lithography stochastic variation. The amount of variation is a function of the magnitude of the LER (more accurately, all the statistical properties of the LER) and the length of the feature edge. These quantities have been analytically linked to provide an estimate for the minimum line length for both optical and e-beam based overlay metrology. The model results have been compared with experimental results from wafers manufactured at IMEC on both EUV and ArF lithographic processes developed for the 10 nm node, with extrapolation to the 5 nm node.

Keywords: overlay metrology, stochastic effects, Line Edge Roughness, Overlay Mark Fidelity, Kernel3Sigma

1. INTRODUCTION

Accurate and precise edge placement in advanced semiconductor manufacturing relies on overlay metrology from proxies or targets in order to disposition and control the lithographic process. The impact of manufacturing processes on target noise and overlay mark fidelity has been characterized in the past[ii],[iii] but such experimental characterization has not provided a quantitative link to basic lithographic quantities such as line edge roughness (LER). Two pending technology transitions currently underway will likely elevate the relative importance of overlay mark fidelity. Firstly, the transition from high order (HO) wafer level models to CPE (correction per exposure) models drastically reduces the ratio of correctables to number of sites from which the model terms are determined. This necessarily means that the impact of any stochastic variations at each individual measurement site will have significantly higher impact on the model correctables. Secondly, the insertion of EUV on a small but critical number of layers is predicted to increase lithographic line edge roughness. The combination of these two effects will potentially conspire to inject significant random noise into the lithographic overlay control loop which, for the 5 nm node, has exceedingly tight requirements. In this investigation we have assessed the impact of LER on optical and SEM overlay mark fidelity and preliminary results indicate that the impact of LER on overlay mark fidelity as characterized by a new metric, normalized kernel 3 sigma, cannot be ruled out.

Metrology, Inspection, and Process Control for Microlithography XXXI, edited by Martha I. Sanchez, Vladimir A. Ukraintsev
Proc. of SPIE Vol. 10145, 1014509 · © 2017 SPIE · CCC code: 0277-786X/17/$18 · doi: 10.1117/12.2258353

Downloaded From: http://proceedings.spiedigitallibrary.org/ on 04/01/2017 Terms of Use: http://spiedigitallibrary.org/ss/termsofuse.aspx

2. MOTIVATION

Consider an overlay target measured across ~550 different wafer locations. The locations are spread across different fields and different intra-field positions, in a way that allows both HO modeling and CPE modeling. Now consider three different stochastic noise levels, normally distributed with mean of zero and different amplitudes, that are added to the targets' overlay across those positions. After 100 iterations the correctables and residuals are determined and compared with the unperturbed results.

Since the HO model averages the effect of the noise across wafer, its correctable terms remain stable across the different noise levels. However, the CPE, which models every field independently, suffers greatly and results in biased corrections, as shown in Figure 1.

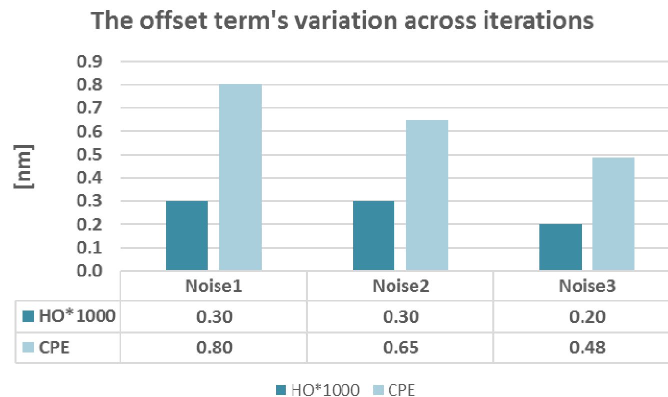

	Noise1	Noise2	Noise3
HO*1000	0.30	0.30	0.20
CPE	0.80	0.65	0.48

Figure 1: Variation across 100 random simulations: while the noise was averaged out in the HO model, the CPE model suffers from the additional random noise in a way that affects its correctable terms

With respect to modeled residuals, as shown in Figure 2, the result is the contrary whereby the noise contribution to the HO case is much higher than to the CPE case, considering that the contribution is in quadrature.

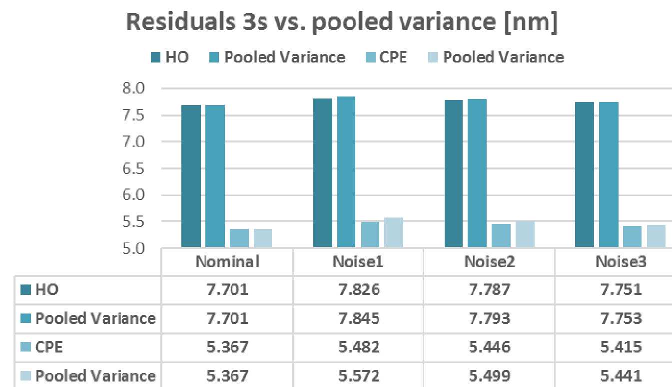

	Nominal	Noise1	Noise2	Noise3
HO	7.701	7.826	7.787	7.751
Pooled Variance	7.701	7.845	7.793	7.753
CPE	5.367	5.482	5.446	5.415
Pooled Variance	5.367	5.572	5.499	5.441

Figure 2: Residuals 3σ of both HO & CPE models vs. pooled variance of the models' residuals and added noise. It can be seen that all of the noise in the HO model goes straight into the residuals while for the CPE model, some of the noise goes into the correctable terms

Downloaded From: http://proceedings.spiedigitallibrary.org/ on 04/01/2017 Terms of Use: http://spiedigitallibrary.org/ss/termsofuse.aspx

3. EXPERIMENTAL METHOD

Wafer processing

Wafers as described in this paper were processed using a modification of the imec N10 BEOL short loop test vehicle, which has been described earlier[iv]. The stack is depicted in Figure 3. Briefly, a triple hardmask (SiO_2 / TiN / SiO_2) is patterned using a negative tone development resist, exposed on an ASML NXT:1950i interfaced with a Sokudo DUO track and dry etched using a Tokyo Electron TACTRAS etcher. Since the objective of this study is to investigate the effect of stochastics on the current layer, the readout of the previous layer was optimized. For this purpose (and in contrast to the standard flavor of this flow), the previous layer was patterned into the TiN (instead of the SiO_2) hardmask, since the TiN patterns result in superior contrast for the optical inspections.

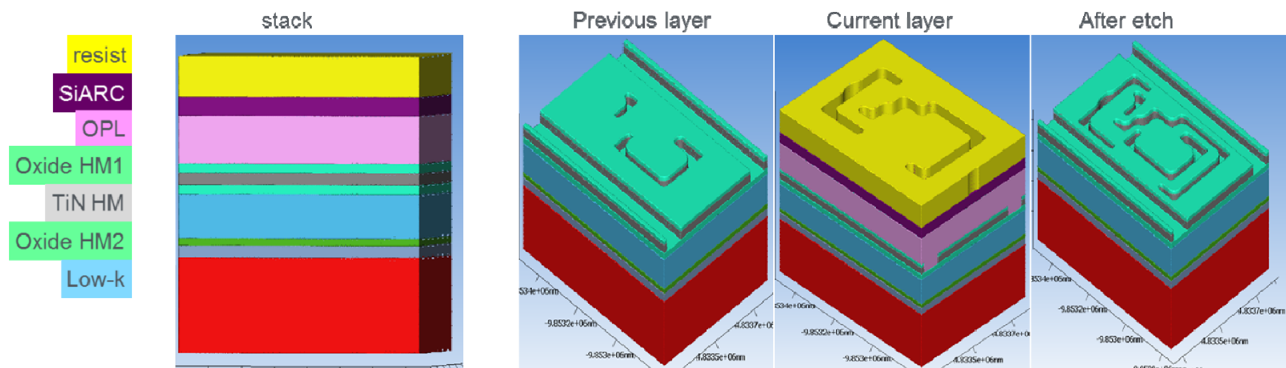

Figure 3 Stack (left) and relevant patterning steps as employed in this study.

For 193nm immersion lithography, the current layer was imaged using a negative tone development resist process with underlying SiARC + OPL on top of the previous layer, using the same cluster as for the previous layer. For EUV lithography, the current layer was imaged using a positive tone EUV resist process with underlying SiARC + OPL on top of the previous layer, using an ASML NXE:3300B interfaced with a Tokyo Electron LITHIUS ProZ track.

Metrology data collection

Line edge and line width roughness were characterized from scanning electron microscopy (SEM) images from a Hitachi CG5000 CD-SEM. Images were collected using rectangular scan mode (field size: 0.675 x 2.562 μm^2). Specifically for the characterization in resist, care was taken to minimize effects of e-beam induced resist shrinkage (and smoothing). Roughness parameters, including power spectral density (PSD) curves, were extracted through off-line image processing using LERDEMO software from Demokritos[v] and MetroLER from Fractilia.

Optical images were collected using an Archer500LCM in single grab mode. Automated recipe setup was used for each layer stack (ArF vs EUV) and for each target type. Images were analyzed using off-line analysis software for determining accuracy of current and previous layer signal.

4. DATA PROCESSING

Line Edge Roughness Analysis

Roughness measurements (line-edge roughness, linewidth roughness, and pattern placement roughness) are generally done on very long lines (> 2 microns) to approximate infinitely long lines. Most commonly, only

Downloaded From: http://proceedings.spiedigitallibrary.org/ on 04/01/2017 Terms of Use: http://spiedigitallibrary.org/ss/termsofuse.aspx

the 3σ roughness (three times the standard deviation of the linewidth measurements along the line for the case of LWR) is reported. While important, this single measure does not contain enough information to enable predictions about the impact of roughness on shorter lines. In particular, the LWR of an infinitely long line will partition into two separate problems for shorter lines of length L: the within-feature variation (σ_{LWR}(L), the LWR of the short line) and feature-to-feature variation (σ_{CDU}(L), the local critical dimension uniformity caused by the roughness). This same partitioning occurs for line-edge roughness and pattern placement roughness. The partitioning can be described by a "conservation of roughness" formula:

$$\sigma_{LWR}^2(\infty) = \sigma_{LWR}^2(L) + \sigma_{CDU}^2(L) \tag{1}$$

But how does this partition of error vary as a function of line length L? A simple measurement of the 3σ roughness does not provide enough information to answer this question. Rather, a full power spectral density (PSD) analysis is required. As has been previously reported, [vi] the local CDU caused by roughness can be related to the PSD parameters by

$$\sigma_{CDU}(L) = \sqrt{\frac{PSD(0)}{L}\left[1 - \frac{\xi}{L}(1 - e^{-L/\xi})\right]} \tag{2}$$

where $PSD(0)$ is the with zero-frequency value of the LWR PSD and ξ is the correlation length. Thus, only by measuring $\sigma_{LWR}(\infty)$, $PSD(0)$, and ξ can one make predictions about how the total roughness for a long line partitions between within-feature and feature-to-feature variation for a shorter line. This partitioning will be needed for the analysis presented below.

Kernel 3sigma Analysis

Imaging Based Overlay (IBO) relies on the determination of the center of symmetry X_c of the images of the structures (e.g., periodic grating) constituting the overlay mark, Figure 4. This center of symmetry can be found by looking for the maximum of the auto-convolution function of the image. The region of interest (ROI) shown in Figure 4 selects the structure in the current (resist) layer designated for the overlay measurement in x-direction. The selected image area is projected on the x-axis by averaging over the transverse y-direction to produce a one-dimensional (1D) "kernel". The center of the symmetry of this kernel can be found as a maximum of its auto-convolution. The corresponding procedure is then repeated for the previous layer, to eventually find the overlay between the two.

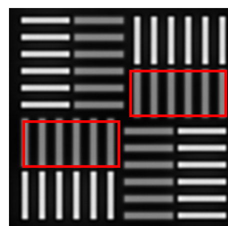

Figure 4 Aim target and regions of interest (ROI) for the current

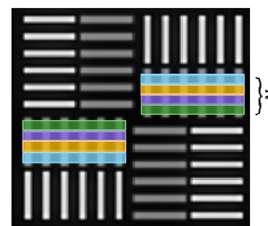

Figure 5 Illustration of the sub-ROI's used for the calculation of

Downloaded From: http://proceedings.spiedigitallibrary.org/ on 04/01/2017 Terms of Use: http://spiedigitallibrary.org/ss/termsofuse.aspx

layer X-direction shown in red. *the K3S.*

The K3S measure is introduced in order to characterize the non-uniformity of the overlay mark. The nominal ROI (Figure 4) is subdivided into N $(\sim 5-10)$ sub-ROI's as shown in Figure 5, which are paired symmetrically (i.e., according to the color in Figure 5). Each sub-region is used to find its own center of the symmetry, which yields N values $\{X_c^i\}_{i=1}^N$, whose variance defines the K3S:

$$K3S = 3 \times STD(X_c^i) \tag{3}$$

With respect to the relationship between K3S and LER, it is anticipated that conditional to meeting the precision lower bound condition and that other contributions are small, then the variance of K3S will be proportional to the LER variance divided by (optical contrast)^2,

$$K3S^2 = \underbrace{N \times Precision^2}_{Lower\ Bound} + A_1 \frac{LER^2}{OC^2} + other\ contributions. \tag{4}$$

We therefore introduce the normalized K3S metric,

$$NK3S = K3S*OC.$$

5. RESULTS

LER results

LER in the AIM marks upon ArF immersion and EUV lithography were compared from rectangular CD-SEM images. Inspections were done in resist and are summarized in Figure 6. Consistently, it is found that the roughness in the EUV printed marks is lower compared to that of the ArF printed marks. This may be counterintuitive, given the roughness challenges for EUV lithography, but should actually not be surprising. First of all, the roughness is proportional to the noise divided by the image gradient. Because of the superior resolution of EUV lithography, compared to ArF immersion, the image log slope is much higher for EUV than for ArF. This has a positive impact on the roughness. Moreover, the segmentation pitches of the AIM marks that are used in this study are quite far from the resolution limit of EUV. Therefore, a relatively high number of photons are available to define each line edge. This also results in lower noise compared to printing near the EUV resolution limit.

Downloaded From: http://proceedings.spiedigitallibrary.org/ on 04/01/2017 Terms of Use: http://spiedigitallibrary.org/ss/termsofuse.aspx

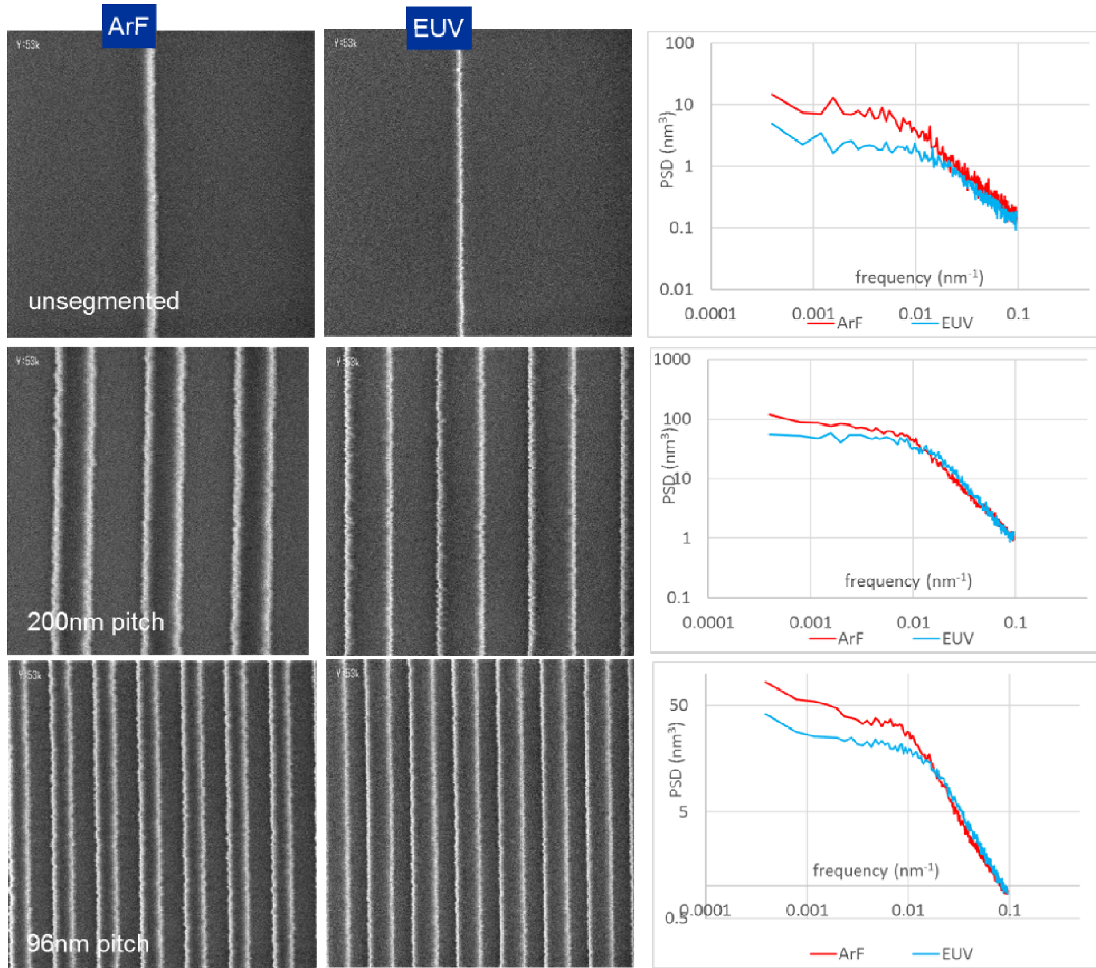

Figure 6 Rectangular CD-SEM images of ArF immersion (left) and EUV (middle) exposed AIM marks (top: unsegmented AIM, middle: AIM mark with 200nm pitch segmentation; bottom: AIM mark with 96nm pitch segmentation). Average PSD curves as calculated from a set (>20).

Upon pattern transfer, roughness may be impacted. There are various mechanisms through which etch can deteriorate roughness. However, in a properly optimized process some smoothing of high and mid frequency roughness may be expected, while low frequency roughness is not impacted. The impact on roughness after transfer of the resist lines into the TiN hard mask is characterized in Figure 7. The shape of the curve is not significantly impacted by the etch process, indicating that no significant smoothing in the mid/high frequency regime occurs. There does appear to be a minor downward shift of the entire curve, indicating overall lower roughness. However, this is likely an artifact of variations in noise of the SEM images.

Downloaded From: http://proceedings.spiedigitallibrary.org/ on 04/01/2017 Terms of Use: http://spiedigitallibrary.org/ss/termsofuse.aspx

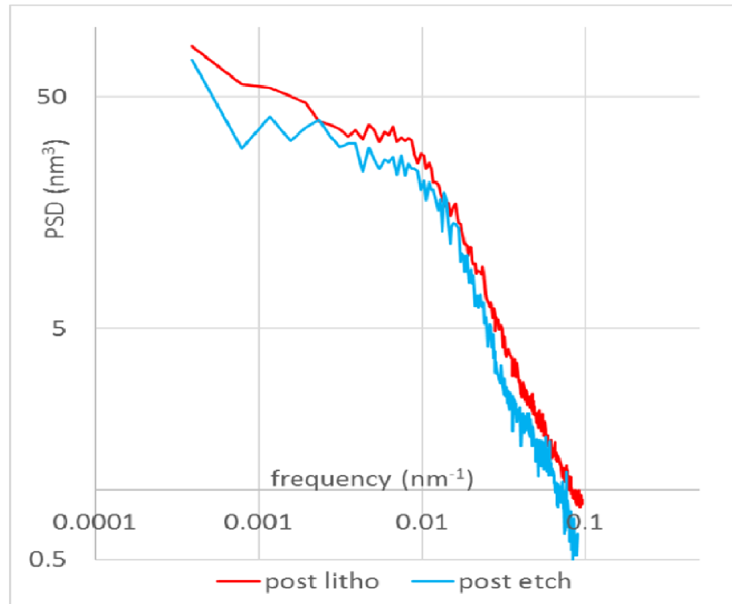

Figure 7 Post-litho (red) and post-etch (blue) PSD curves of 96nm pitch line/space structures exposed with ArF.

Also the impact of dose and focus on roughness has been characterized on the FEM-exposed current layer (Figure 8). As discussed previously, roughness is expected to be inversely proportional to the image gradient (log-slope). Therefore, both dose and focus may be expected to have an impact on LER. Indeed, this can be seen from the results in Figure 8. In under-exposure conditions NILS deteriorates, which would result in increasing LER. This can be seen in the ArF immersion results, where the lowest LER can be found on the right side of the wafer (highest dose). However, the LER signature through focus is typically more pronounced as indeed is also observed in the data. Best focus in the EUV wafers is easily determined from the LER at row+3. The ArF data also shows through focus variation of the LER, but in this case the best focus position depends on the feature size. Such pitch dependent best focus is attributed to Bossung tilts that are frequently observed near the ultimate resolution as a consequence of mask 3D effects[vii].

Downloaded From: http://proceedings.spiedigitallibrary.org/ on 04/01/2017 Terms of Use: http://spiedigitallibrary.org/ss/termsofuse.aspx

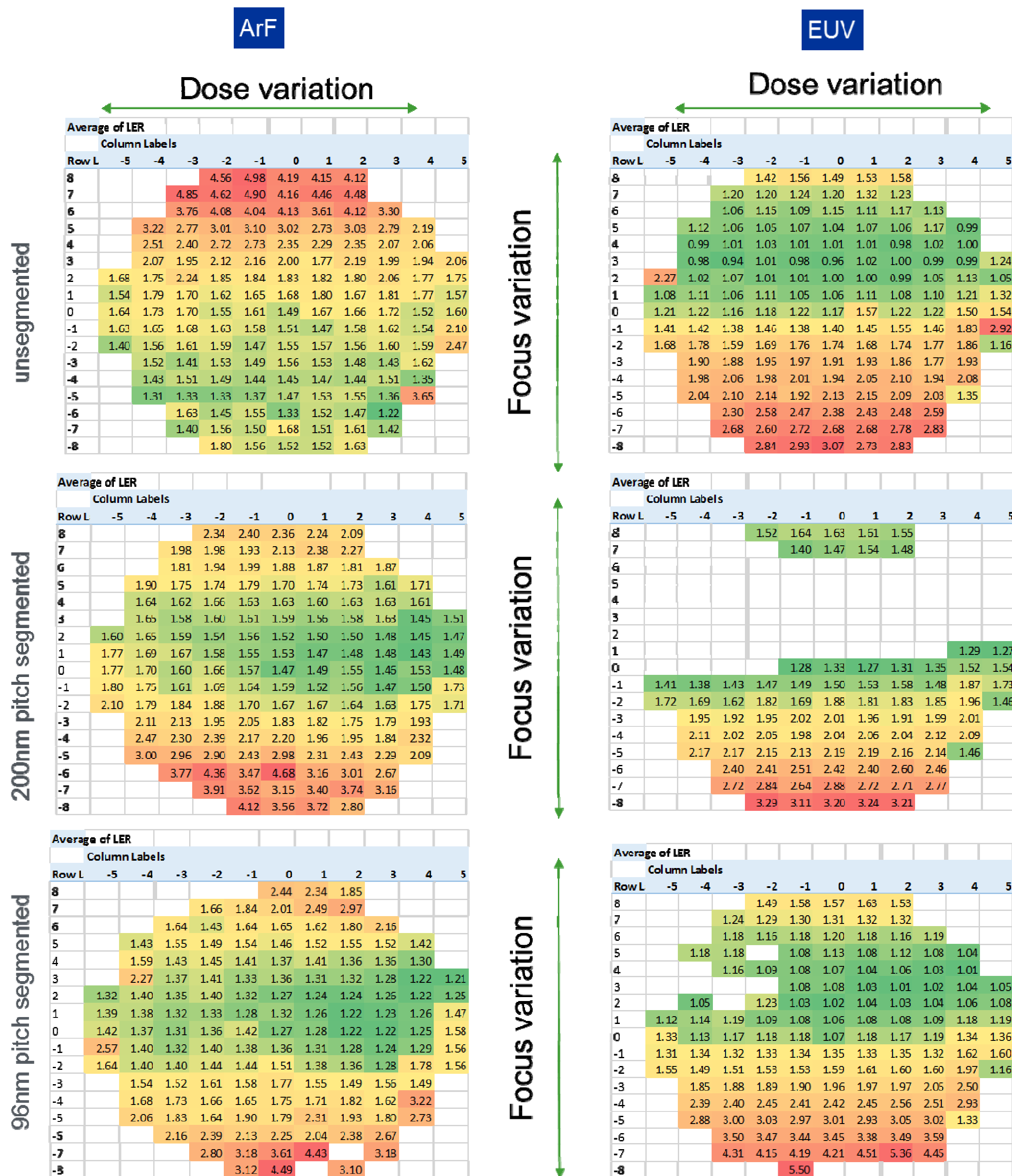

ArF – unsegmented

Average of LER

Row L	-5	-4	-3	-2	-1	0	1	2	3	4	5
8				4.56	4.98	4.19	4.15	4.12			
7			4.85	4.62	4.90	4.16	4.46	4.48			
6			3.76	4.08	4.04	4.13	3.61	4.12	3.30		
5		3.22	2.77	3.01	3.10	3.02	2.73	3.03	2.79	2.19	
4		2.51	2.40	2.72	2.73	2.35	2.29	2.35	2.07	2.06	
3		2.07	1.95	2.12	2.16	2.00	1.77	2.19	1.99	1.94	2.06
2	1.68	1.75	2.24	1.85	1.84	1.83	1.82	1.80	2.06	1.77	1.75
1	1.54	1.79	1.70	1.62	1.65	1.68	1.80	1.67	1.81	1.77	1.57
0	1.64	1.73	1.70	1.55	1.61	1.49	1.67	1.66	1.72	1.52	1.60
-1	1.63	1.65	1.68	1.63	1.58	1.51	1.47	1.58	1.62	1.54	2.10
-2	1.40	1.56	1.61	1.59	1.47	1.55	1.57	1.56	1.60	1.59	2.47
-3		1.52	1.41	1.53	1.49	1.56	1.53	1.48	1.43	1.62	
-4		1.43	1.51	1.49	1.44	1.45	1.47	1.44	1.51	1.35	
-5		1.31	1.33	1.33	1.37	1.47	1.53	1.55	1.36	3.65	
-6			1.63	1.45	1.55	1.33	1.52	1.47	1.22		
-7			1.40	1.56	1.50	1.68	1.51	1.61	1.42		
-8				1.80	1.56	1.52	1.52	1.63			

EUV – unsegmented

Average of LER

Row L	-5	-4	-3	-2	-1	0	1	2	3	4	5
8				1.42	1.56	1.49	1.53	1.58			
7			1.20	1.20	1.24	1.20	1.32	1.23			
6			1.06	1.15	1.09	1.15	1.11	1.17	1.13		
5		1.12	1.06	1.05	1.07	1.04	1.07	1.06	1.17	0.99	
4		0.99	1.01	1.03	1.01	1.01	1.01	0.98	1.02	1.00	
3		0.98	0.94	1.01	0.98	0.96	1.02	1.00	0.99	0.99	1.24
2	2.27	1.02	1.07	1.01	1.01	1.00	1.00	0.99	1.05	1.13	1.05
1	1.08	1.11	1.06	1.11	1.05	1.06	1.11	1.08	1.10	1.21	1.32
0	1.21	1.22	1.16	1.18	1.22	1.17	1.57	1.22	1.22	1.50	1.54
-1	1.41	1.42	1.38	1.46	1.38	1.40	1.45	1.55	1.46	1.83	2.92
-2	1.68	1.78	1.59	1.69	1.76	1.74	1.68	1.74	1.77	1.86	1.16
-3		1.90	1.88	1.95	1.97	1.91	1.93	1.86	1.77	1.93	
-4		1.98	2.06	1.98	2.01	1.94	2.05	2.10	1.94	2.08	
-5		2.04	2.10	2.14	1.92	2.13	2.15	2.09	2.03	1.35	
-6			2.30	2.58	2.47	2.38	2.43	2.48	2.59		
-7			2.68	2.60	2.72	2.68	2.68	2.78	2.83		
-8				2.81	2.93	3.07	2.73	2.83			

ArF – 200nm pitch segmented

Average of LER

Row L	-5	-4	-3	-2	-1	0	1	2	3	4	5
8				2.34	2.40	2.36	2.24	2.09			
7			1.98	1.98	1.93	2.13	2.38	2.27			
6			1.81	1.94	1.99	1.88	1.87	1.81	1.87		
5		1.90	1.75	1.74	1.79	1.70	1.74	1.73	1.61	1.71	
4		1.64	1.62	1.66	1.53	1.63	1.60	1.63	1.63	1.61	
3		1.65	1.58	1.60	1.51	1.59	1.56	1.58	1.63	1.45	1.51
2	1.60	1.65	1.59	1.54	1.56	1.52	1.50	1.50	1.48	1.45	1.47
1	1.77	1.69	1.67	1.58	1.55	1.53	1.47	1.48	1.48	1.43	1.49
0	1.77	1.70	1.60	1.66	1.57	1.47	1.49	1.55	1.45	1.53	1.48
-1	1.80	1.75	1.61	1.69	1.64	1.59	1.52	1.56	1.47	1.50	1.73
-2	2.10	1.79	1.84	1.88	1.70	1.67	1.67	1.64	1.63	1.75	1.71
-3		2.11	2.13	1.95	2.05	1.83	1.82	1.75	1.79	1.93	
-4		2.47	2.30	2.39	2.17	2.20	1.96	1.95	1.84	2.32	
-5		3.00	2.96	2.90	2.43	2.98	2.31	2.43	2.29	2.09	
-6			3.77	4.36	3.47	4.68	3.16	3.01	2.67		
-7				3.91	3.52	3.15	3.40	3.74	3.15		
-8					4.12	3.56	3.72	2.80			

EUV – 200nm pitch segmented

Average of LER

Row L	-5	-4	-3	-2	-1	0	1	2	3	4	5
8				1.52	1.64	1.63	1.51	1.55			
7					1.40	1.47	1.54	1.48			
6											
5											
4											
3											
2											
1										1.29	1.27
0					1.28	1.33	1.27	1.31	1.35	1.52	1.54
-1	1.41	1.38	1.43	1.47	1.49	1.50	1.53	1.58	1.48	1.87	1.73
-2	1.72	1.69	1.62	1.82	1.69	1.88	1.81	1.83	1.85	1.96	1.46
-3		1.95	1.92	1.95	2.02	2.01	1.96	1.91	1.99	2.01	
-4		2.11	2.02	2.05	1.98	2.04	2.06	2.04	2.12	2.09	
-5		2.17	2.17	2.15	2.13	2.19	2.19	2.16	2.14	1.46	
-6			2.40	2.41	2.51	2.42	2.40	2.60	2.46		
-7			2.72	2.84	2.64	2.88	2.72	2.71	2.77		
-8				3.29	3.11	3.20	3.24	3.21			

ArF – 96nm pitch segmented

Average of LER

Row L	-5	-4	-3	-2	-1	0	1	2	3	4	5
8						2.44	2.34	1.85			
7				1.66	1.84	2.01	2.49	2.97			
6			1.64	1.43	1.64	1.65	1.62	1.80	2.16		
5		1.43	1.55	1.49	1.54	1.46	1.52	1.55	1.52	1.42	
4		1.59	1.43	1.45	1.41	1.37	1.41	1.36	1.36	1.30	
3		2.27	1.37	1.41	1.33	1.36	1.31	1.32	1.28	1.22	1.21
2	1.32	1.40	1.35	1.40	1.32	1.27	1.24	1.24	1.26	1.22	1.25
1	1.39	1.38	1.32	1.33	1.28	1.32	1.26	1.22	1.23	1.26	1.47
0	1.42	1.37	1.31	1.36	1.42	1.27	1.28	1.22	1.22	1.25	1.58
-1	2.57	1.40	1.32	1.40	1.38	1.36	1.31	1.28	1.24	1.29	1.56
-2	1.64	1.40	1.40	1.44	1.44	1.51	1.38	1.36	1.28	1.78	1.56
-3		1.54	1.52	1.61	1.58	1.77	1.55	1.49	1.56	1.49	
-4		1.68	1.73	1.66	1.65	1.75	1.71	1.82	1.62	3.22	
-5		2.06	1.83	1.64	1.90	1.79	2.31	1.93	1.80	2.73	
-5			2.16	2.39	2.13	2.25	2.04	2.38	2.67		
-7				2.80	3.18	3.61	4.43		3.18		
-8					3.12	4.49		3.10			

EUV – 96nm pitch segmented

Average of LER

Row L	-5	-4	-3	-2	-1	0	1	2	3	4	5
8				1.49	1.58	1.57	1.63	1.53			
7			1.24	1.29	1.30	1.31	1.32	1.32			
6			1.18	1.15	1.18	1.20	1.18	1.16	1.19		
5		1.18	1.18		1.08	1.13	1.08	1.12	1.08	1.04	
4			1.16	1.09	1.08	1.07	1.04	1.06	1.03	1.01	
3					1.08	1.08	1.03	1.01	1.02	1.04	1.05
2		1.05		1.23	1.03	1.02	1.04	1.03	1.04	1.06	1.08
1	1.12	1.14	1.19	1.09	1.08	1.06	1.08	1.08	1.09	1.18	1.19
0	1.33	1.13	1.17	1.18	1.18	1.07	1.18	1.17	1.19	1.34	1.36
-1	1.31	1.34	1.32	1.33	1.34	1.35	1.33	1.35	1.32	1.62	1.60
-2	1.55	1.49	1.51	1.53	1.53	1.59	1.61	1.60	1.60	1.97	1.16
-3		1.85	1.88	1.89	1.90	1.96	1.97	1.97	2.05	2.50	
-4		2.39	2.40	2.45	2.41	2.42	2.45	2.56	2.51	2.93	
-5		2.88	3.00	3.03	2.97	3.01	2.93	3.05	3.02	1.33	
-6			3.50	3.47	3.44	3.45	3.38	3.49	3.59		
-7			4.31	4.15	4.19	4.21	4.51	5.36	4.45		
-8					5.50						

Figure 8 1σ LER data of AIM marks in the current layer across wafer exposed with ArF immersion (left) and EUV (right) lithography. Note that a Focus-Exposure matrix layout has been used. Top: unsegmented AIM, middle: AIM mark with 200nm pitch segmentation; bottom: AIM mark with 96nm pitch segmentation. Data from 200nm segmented targets at EUV is missing due to data acquisition setup.

AIM K3S results

Below we give the experimental results for K3S versus the LER:

Downloaded From: http://proceedings.spiedigitallibrary.org/ on 04/01/2017 Terms of Use: http://spiedigitallibrary.org/ss/termsofuse.aspx

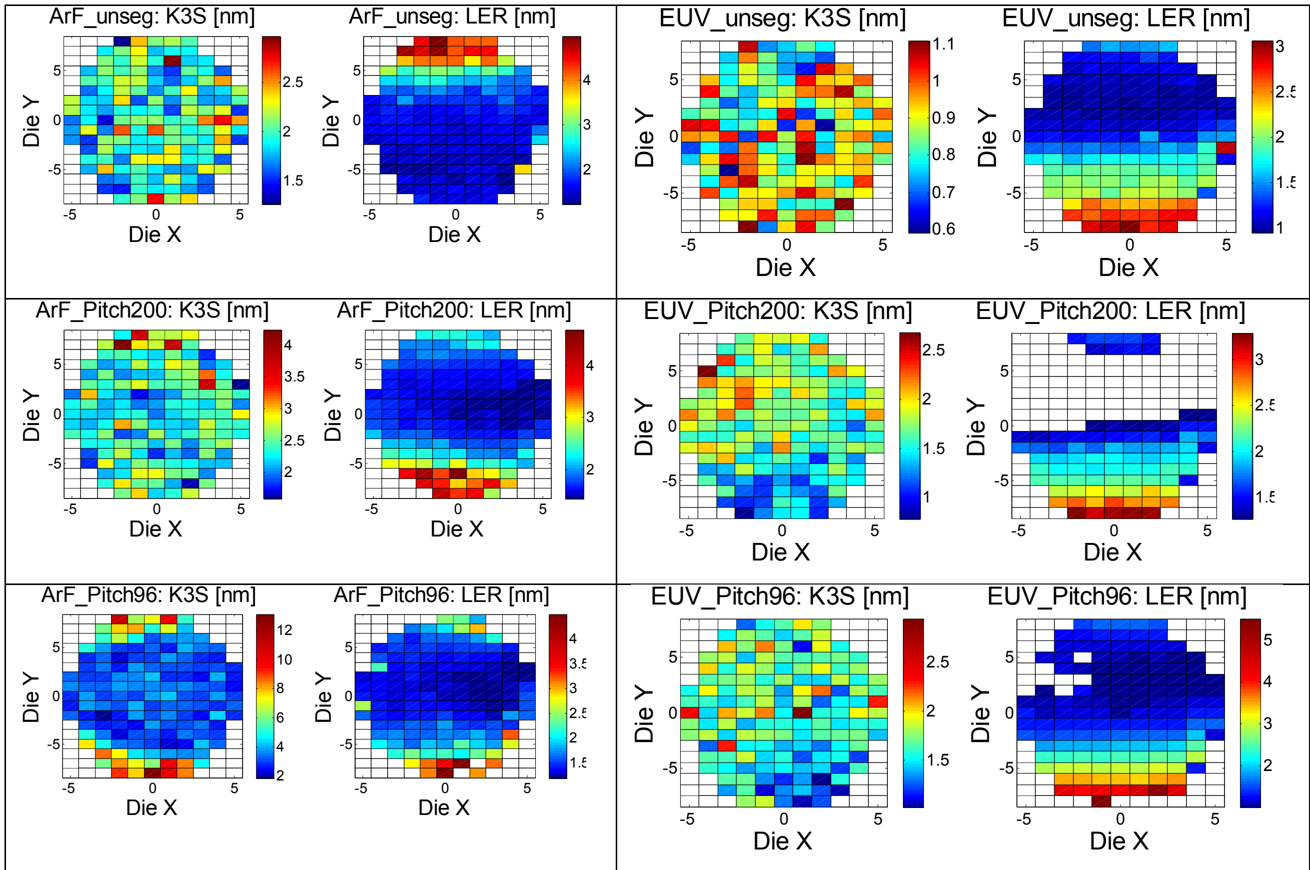

Table 1: ArF (left) and EUV (right) Kernel 3sigma and LER wafer maps, side by side. No significant correlation is observed.

Below we give the experimental results for K3S normalized by the contrast versus the LER

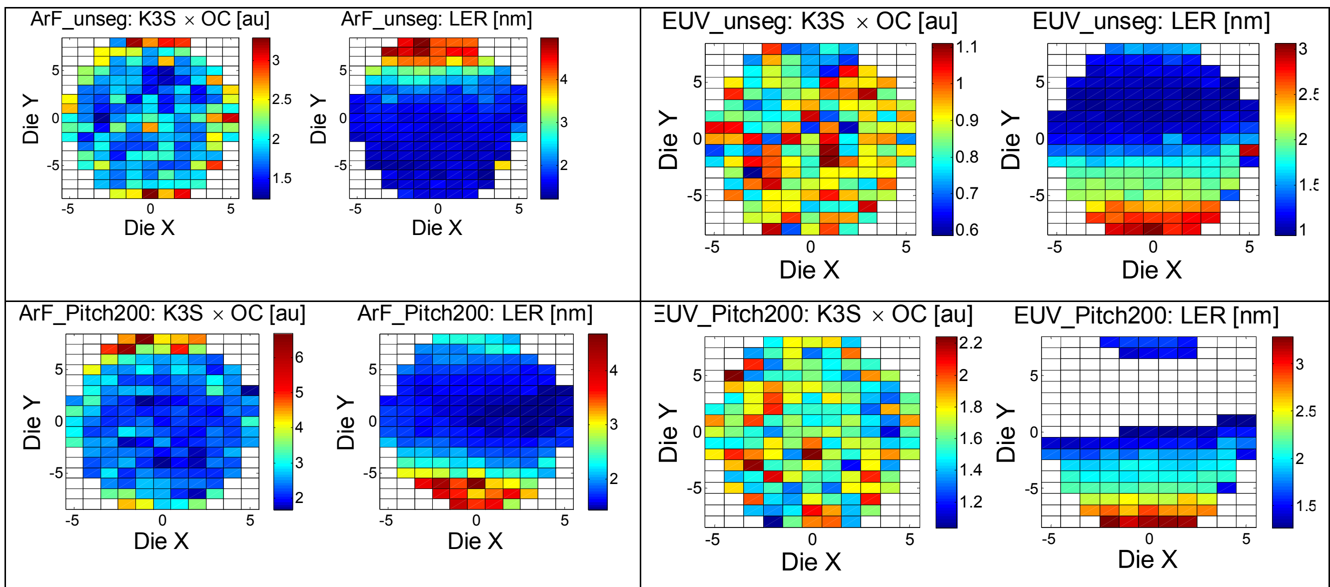

Downloaded From: http://proceedings.spiedigitallibrary.org/ on 04/01/2017 Terms of Use: http://spiedigitallibrary.org/ss/termsofuse.aspx

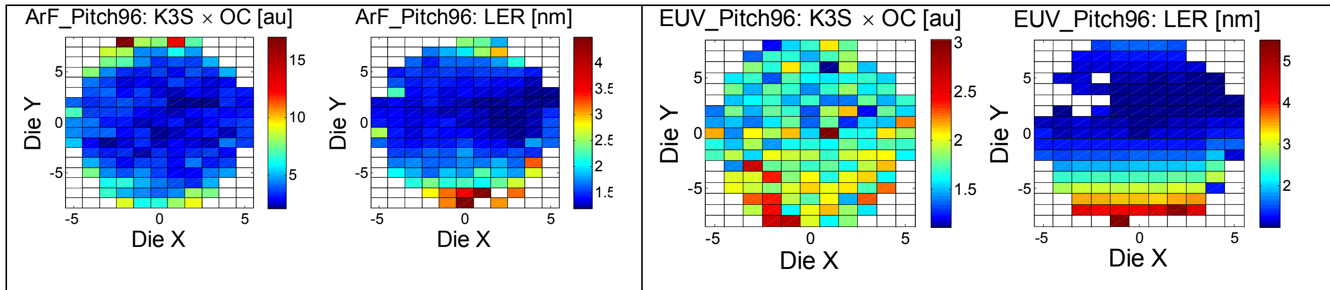

Table 2: ArF (left) and EUV (right) normalized Kernel 3sigma and LER wafer maps, side by side. For 96 nm segmentation pitch some correlation is observed.

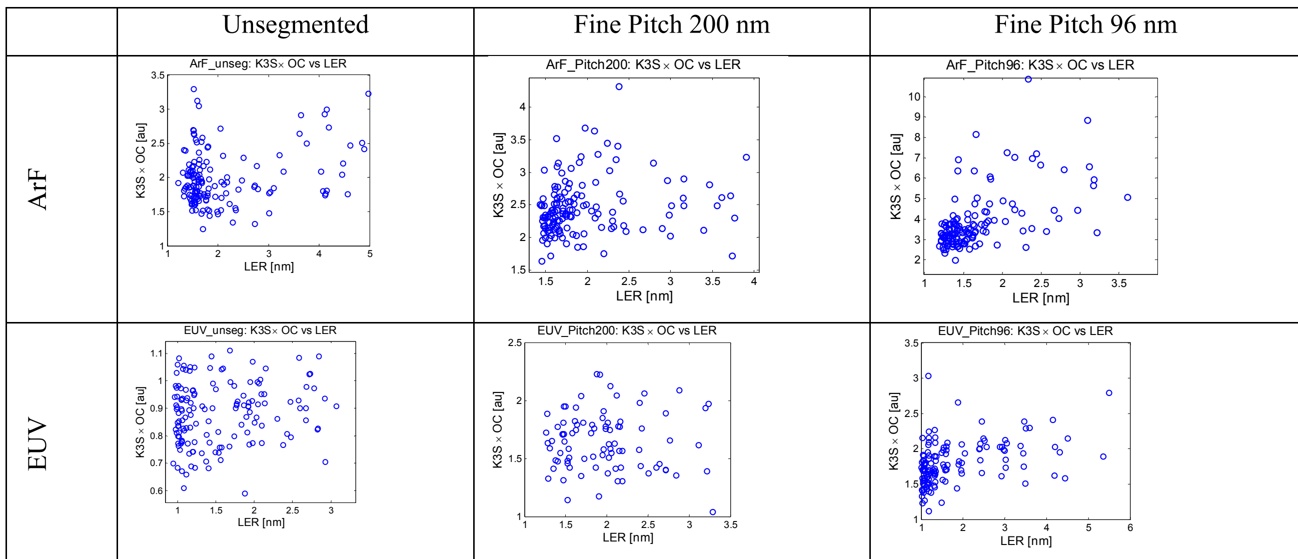

Table 3: Correlation scatter plots of LER vs NK3S for ArF and EUV lithography and different target segmentations.

6. DISCUSSION

Minimum edge length requirements

What line length is required so that the stochastic contribution to pattern placement error for that line is less than a specified amount? This question is similar to the question of how linewidth roughness contributes to critical dimension uniformity of a line of length L (that is, the local CDU), a problem that has been previous addressed.[vi] Consider a typical pattern placement roughness (PPR) power spectral density (PSD) with zero-frequency value $PSD(0)$ and correlation length ξ. The uncertainty in the mean center position of a line of length L will be

$$\sigma_{PPE} = \sqrt{\frac{PSD(0)}{L}\left[1-\frac{\xi}{L}\left(1-e^{-L/\xi}\right)\right]} \tag{5}$$

Downloaded From: http://proceedings.spiedigitallibrary.org/ on 04/01/2017 Terms of Use: http://spiedigitallibrary.org/ss/termsofuse.aspx

Let PPE_{spec} be the 3σ specification for the maximum allowable stochastic contribution to pattern placement error per layer. A typical value for PPE_{spec} might be 0.2 nm for state of the art overlay metrology. Then, we look for the line length L that produces a 3σ pattern placement uncertainty of this amount. Since that line length will be much greater than the correlation length, equation (5) simplifies and the needed line length becomes

$$L = \frac{9PSD(0)}{\left(PPE_{spec}\right)^2} \tag{6}$$

As an example, consider the case where the PSD of the PPR has $PSD(0) = 10$ nm^3. For a PPE spec of 0.2 nm, the needed line length is 2.25 μm. Note that since typical correlation lengths are on the order of 10 – 20 nm, the approximation the $L >> \xi$ is a good one for this application.

Turning now to the specific examples from the data sets in the current work, the PSD(0) was calculated with no image filtering and edge detection was performed by the Analytical Linescan Model. Note that these PSD(0) values are generally lower than those shown in section 5 as these are the PPR PSDs.

Table 4: Analysis of the pattern placement roughness leads to predictions of the minimum line length required to meet a given pattern placement error specification.

Pattern Placement Roughness	previous (ArF, post-etch)	Current (EUV, ADI)	Current (ArF, ADI)
Biased 3-sigma (nm)	2.0	2.3	2.3
Unbiased 3-sigma (nm)	1.6	1.8	1.9
PSD(0) (nm^3)	13.0	10.9	16.0
Correlation Length (nm)	22.5	15.4	19.8
SIOE (nm)	0.12	0.12	0.12
L_{min} (μm)	8.1	6.8	10.0

Downloaded From: http://proceedings.spiedigitallibrary.org/ on 04/01/2017 Terms of Use: http://spiedigitallibrary.org/ss/termsofuse.aspx

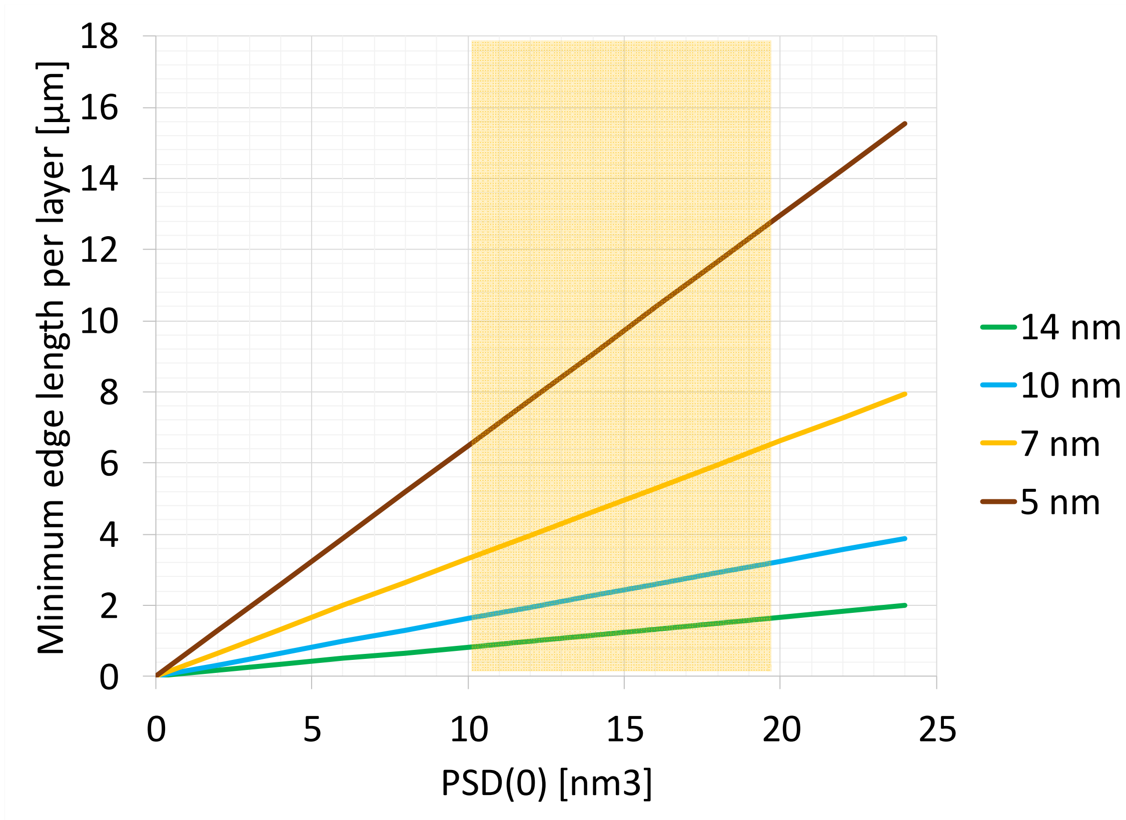

Figure 9 Minimum edge length requirements as a function of PSD(0) for different technology nodes. The shaded region indicates levels of PSD(0) for metrology target structures evaluated in this publication.

For SEM overlay metrology, edge length requirements of 1 – 3 µm are typical of the 10 – 14 nm nodes in use today. However, as we approach the 7 and 5 nm nodes, these length requirements will increase significantly to 6 – 12 µm per layer. Furthermore this assumes that the PSD(0) numbers will be maintained for EUV lithography. However, as we approach the minimum design rule pitches of ~ 24 nm it is anticipated that these numbers will degrade as the normalized image log slope is reduced as discussed in section 4.

Optical overlay implications

Turning now to the LER vs K3S correlation analysis we first note that the observed K3S is well above the precision lower bound. Secondly, we observe no significant correlation between the two measured quantities for any of the target or lithography permutations. However, for segmented targets some correlation between LER and NK3S is observed as defined in section 4 above. Additionally, since the FEM matrix was not randomized, it cannot be ruled out that this correlation is spatial in nature and results from a shared correlation to a third focus/dose dependent quantity.

7. CONCLUSIONS

As overlay control loops transition from W3F3 to CPE overlay models, the model term sensitivity to stochastic variations frozen into the overlay metrology target becomes more significant. LER and PSD of unsegmented and DR segmented overlay metrology targets have been characterized from SEM images. It is

Downloaded From: http://proceedings.spiedigitallibrary.org/ on 04/01/2017 Terms of Use: http://spiedigitallibrary.org/ss/termsofuse.aspx

observed that compared with ArF, EUV lithography shows a reduction in LER and PSD for the segmentation sizes measured. This conclusion is by no means universal and is probably the result of the excellent normalized image log slope obtained with EUV lithography at this feature size. Upon review of the PSD data, it is observed that the spectral content of the LER at optically resolvable spatial frequencies is non-negligible. Kernel 3 sigma is introduced as a metric of stochastic noise contributors to optical imaging overlay mark fidelity. For segmented targets, some correlation is observable between LER & NK3S, however, a randomized FEM should be used to decouple other systematic location dependent effects which maybe responsible for this correlation.

Finally, it is asserted that LER contributes directly to overlay metrology and a minimum target size criterion is proposed in units of line-length L per layer, as given above in equation (6). This criterion is easily met by optical metrology but should be carefully considered for SEM overlay metrology.

8. REFERENCES

[i] Chris A. Mack ; James W. Thackeray ; John J. Biafore and Mark D. Smith, "Stochastic exposure kinetics of EUV photoresists: a simulation study", Proc. SPIE 7969, Extreme Ultraviolet (EUV) Lithography II, 796919 (April 06, 2011); doi:10.1117/12.881066.

[ii] Mike Adel ; Mark Ghinovker ; Jorge M. Poplawski ; Elyakim Kassel ; Pavel Izikson, Ivan K. Pollentier ; Philippe Leray ; David W. Laidler, "Characterization of overlay mark fidelity", Proc. SPIE 5038, Metrology, Inspection, and Process Control for Microlithography XVII, 437 (May 27, 2003)doi: 10.1117/12.483430.

[iii] Joel L. Seligson ; Mike E. Adel ; Pavel Izikson ; Vladimir Levinski and Dan Yaffe, "Target noise in overlay metrology", Proc. SPIE 5375, Metrology, Inspection, and Process Control for Microlithography XVIII, 403 (May 24, 2004)doi: 10.1117/12.534515.

[iv] P. Leray, M. Mao, B. Baudemprez, N. Amir "Overlay metrology solutions in a triple patterning scheme" *Proc. SPIE*, 9424, (2015), 92420E.

[v] V. Constantoudis, G. P. Patsis, E. Gogolides "Correlation length and the problem of Line Width Roughness" *Proc. SPIE*, 6518, (2007), 65181N.

[vi] Chris A. Mack, "Analytical Expression for Impact of Linewidth Roughness on Critical Dimension Uniformity", *Journal of Micro/Nanolithography, MEMS, and MOEMS*, **13**(2), 020501 (2014).

[vii] S. Suh, S. J. Lee, K.-y. Back, S. Lee, Y. Kim, S. Kim, Y.-J. Chun "Three-dimensional mask effect approximate modeling for sub-50-nm node device OPC" *Proc. SPIE*, 6521, (2007), 652103.

Downloaded From: http://proceedings.spiedigitallibrary.org/ on 04/01/2017 Terms of Use: http://spiedigitallibrary.org/ss/termsofuse.aspx